Lecture 6: Microstructural studies

E. J. Hinch

1 Deformable Microstructure

All of the microstructural elements discussed so far have been rigid. Most real non-Newtonian fluids are composed of deformable bodies, such as liquid drops or flexible polymers. Allowing deformable microstructure dramatically increases the complexity of the problem because the microstructure now has a large number of internal degrees of freedom. We will first consider the case of dilute suspensions where the interactions between the microscopic particles can be ignored.

1.1 Emulsions

One of simplest fluids with a deformable microstructure is an emulsion of immiscible drops in a solvent. Let the emulsion consist of drops of fluid with viscosity μ_{in}, surface tension T, and characteristic radius a suspended in a solvent with viscosity μ_{out} (μ_{out} is the viscosity of the external fluid). The drops are dilute, non-interacting, and do not mix with the exterior fluid.

Suppose that the drop is caught in a purely straining flow with strain rate E. The straining flow exerts a viscous stress $\mu_{\text{out}}E$ that stretches the drop. This stress is counteracted by the drop's surface tension T/a which tends to make the drop spherical. The equilibrium shape is somewhat sausage-like, as shown in Figure 1. If the viscous stress on the drop exceeds its capillary pressure, that is if $\mu_{\text{out}}E > T/a$, the drop will (normally) rupture. Each rupture reduces the size of the drops, which drives up the capillary pressure. This rupturing process will halt when the drops reach the radius

$$a_* = \frac{T}{\mu_{\text{out}}E}. \tag{1}$$

The size reduction is essentially irreversible since coalescence is usually much slower than the time scale of the exterior flow.

Rupture is difficult if the internal viscosity is too large or too small compared to the external viscosity. If $\mu_{\text{in}} \ll \mu_{\text{out}}$ the drops are too slippery for the exterior flow to have a strong effect. Theoretical and experimental estimates indicate that the drops become long

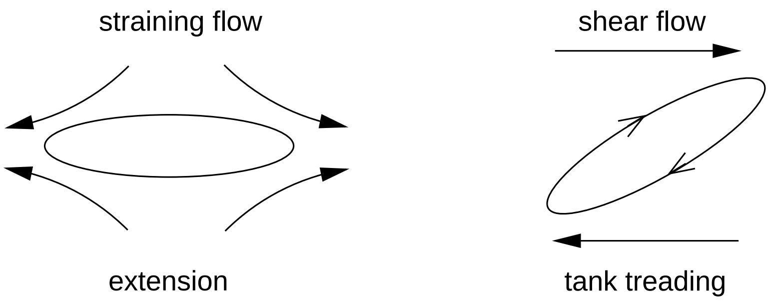

Figure 1: Pre-rupture shapes of drops in an emulsion in straining and shearing flow.

and thin, but do not rupture unless

$$\mu_{\text{out}} E > \frac{T}{a} \begin{cases} 0.54 \left(\dfrac{\mu_{\text{out}}}{\mu_{\text{in}}} \right)^{2/3} & \text{simple shear} \\ 0.14 \left(\dfrac{\mu_{\text{out}}}{\mu_{\text{in}}} \right)^{1/6} & \text{extensional flow} \end{cases} \tag{2}$$

However, mobile surfactants in the drop will give the exterior flow something to grab onto and causes the drops to lose small droplets off their pointed ends. This phenomenon, called 'tip-streaming,' occurs if $\mu_{\text{out}} E > 0.56\, T/a$.

In general, the dimensionless capillary number

$$\mathrm{Ca} = \frac{T}{a \mu_{\text{out}} E} \tag{3}$$

measures the efficiency of an emulsification process. For simple straining flows and viscosity ratios in the range

$$10^{-2} \lesssim \frac{\mu_{\text{in}}}{\mu_{\text{out}}} \lesssim 1, \tag{4}$$

the capillary number is near unity, but it can be as large as 20 for viscosity ratios outside this range.

A shear flow will induce internal circulation in the drops. In the limit of very small internal viscosity, all of the external vorticity is taken up by the internal circulation and the envelope will not rotate relative to the external flow (Figure 1). This phenomenon is known as 'tank treading' because the fluid on the drop surface is stationary relative to the fluid just outside the surface, just as a tank's treads are stationary relative to the ground. As the internal viscosity increases, more and more of the external vorticity is taken up by solid body rotation of the drop.

Shear flow will cause extension of the drops just as in straining flow, and the conditions for rupture and the final drop size as similar to the previous case. One crucial difference is that shear flow cannot rupture the drops if $\mu_{\text{in}} > 3\mu_{\text{out}}$. If this is the case, the drops are so rigid that they just rotate with the exterior vorticity. The drops are still extended by the exterior flow, but before they can rupture they rotate so that they are stretched in the orthogonal direction. Instead of rupturing, the drops are periodically stretched and compressed around their mean shapes.

In order to determine the effect of the drops on the rheology, we have to solve the Stokes problem for both the interior and exterior flow, as well as determine the location of the free surface. This is challenging and not very efficient. To make progress, we consider small ellipsoidal deformations of a spherical drop.

Let the location of the free surface be given by

$$r(\boldsymbol{x},t) = a(1 + \boldsymbol{x}\cdot\mathsf{A}(t)\cdot\boldsymbol{x} + \cdots), \tag{5}$$

where a is the equilibrium radius of the drop. The leading few terms of the evolution equation for the deformation tensor A in Stokes flow are

$$\frac{D\mathsf{A}}{Dt} - \Omega\cdot\mathsf{A} + \mathsf{A}\cdot\Omega = k_1\mathsf{E} + k_5(\mathsf{A}\cdot\mathsf{E} + \mathsf{E}\cdot\mathsf{A}) - \frac{T}{\mu_{\text{out}}a}(k_2\mathsf{A} + k_6\mathsf{A}\cdot\mathsf{A} + \cdots) \tag{6}$$

$$\sigma = -p\mathsf{I} + 2\mu_{\text{out}}\mathsf{E} + 2\mu_{\text{out}}\phi\left[k_3\mathsf{E} + k_7(\mathsf{A}\cdot\mathsf{E} + \mathsf{E}\cdot\mathsf{A}) - \frac{T}{\mu_{\text{out}}a}(k_4\mathsf{A} + k_8\mathsf{A}\cdot\mathsf{A} + \cdots) + \cdots\right]. \tag{7}$$

with coefficients k_n that depend on the viscosity ratio $\lambda = \mu_{\text{in}}/\mu_{\text{out}}$. About 16 of the coefficients have been calculated. The first four are

$$k_1 = \frac{5}{2\lambda+3}, \qquad k_2 = \frac{40(\lambda+1)}{(2\lambda+3)(19\lambda+16)},$$
$$k_3 = \frac{5(\lambda-1)}{2\lambda+3}, \qquad k_4 = \frac{4}{2\lambda+3}.$$

Unfortunately, this theory does not fit the data very well and its restriction to small deformations make it mute on the effect of drop rupture on the rheology.

Experiments and numerical studies have shown that the pre-rupture rheology is characterized by small strain hardening and small shear thinning, with $N_1 > 0$ and $N_2 < 0$. Interestingly, repeated rupture leaves the effective viscosity nearly constant since rupture preserves the volume fraction of the droplets. This is consistent with Einstein's observation that the effective viscosity of a suspension depends only on the volume fraction of the particles and not on their absolute size.

2 Electrical Double Layers

Another deformable microstructure is an electric double layer around a charged colloidal particle. The solvent ions dissociate in presence of charged particles, forming a neutralizing cloud of counter-ions. The thickness of the double layer is given by the Debye length κ^{-1}, where

$$\kappa^2 = \sum_i \frac{n_i Z_i^2 e^2}{\epsilon k T}. \tag{8}$$

Here, $Z_i e$ is the charge on solvent ions of number density n_i and ϵ the dielectric constant. Thus, the colloidal particles act as spheres with a slightly larger radius, contributing a very small increase in the Einstein viscosity. In addition, the flow can distort this cloud but at low concentrations the effect is negligible.

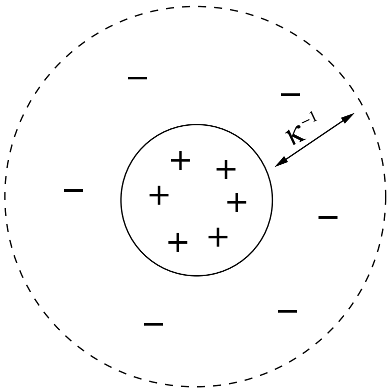

Figure 2: An electric double layer around a charged colloidal particle

3 Interactions

In this section we study the interactions between particles in concentrated solutions. These interactions include excluded volume interactions of rigid spheres and rods as well as deformable drops; electrical and van der Waals interactions.

3.1 Rigid Spheres

For a dilute solution of rigid spheres, only pair interactions (i.e. collisions) are important. At low shear rates, the effect of the collisions is to increase the effective viscosity [1]:

$$\mu^* = \mu(1 + 2.5\varphi + 6.2\varphi^2). \tag{9}$$

The data from experiments by Saunders verifies the above result [2, 3] as shown in Figure 3. (This is Figure 14.17 from [4].) For purely extensional flows, the coefficient of the φ^2 term is 7.6.

For high concentrations, the experiments show shear thinning by a factor of roughly two. The shear thinning effect increases with the concentration. This is illustrated in Figure 4. (This is Figure 14.3 and 14.4(a) from [4].) The numerical simulations show shear thinning at moderate shear rates and shear thickening at high shear rates. This shear thickening has not been verified experimentally and may be a numerical artifact.

3.2 Electrical Interactions

As discussed previously, electrically charged colloids tend to form a shielding cloud of solution counter-ions whose thickness is given by the Debye length κ^{-1}. This cloud has a profound effect on the dynamics of collisions between colloidal particles. If the approaching particles are separated by a length r much greater than the Debye length, the particles interact like uncharged spheres of slightly augmented radius. Once the particle separation becomes comparable to the Debye length, the colloids begin to feel their mutual electrical repulsion. Their approach is halted at a characteristic distance r_*, determined from

$$6\pi\mu a\dot{\gamma}r_* = \frac{\epsilon\zeta a^2\kappa}{r_*}e^{-\kappa(r_*-a)},$$

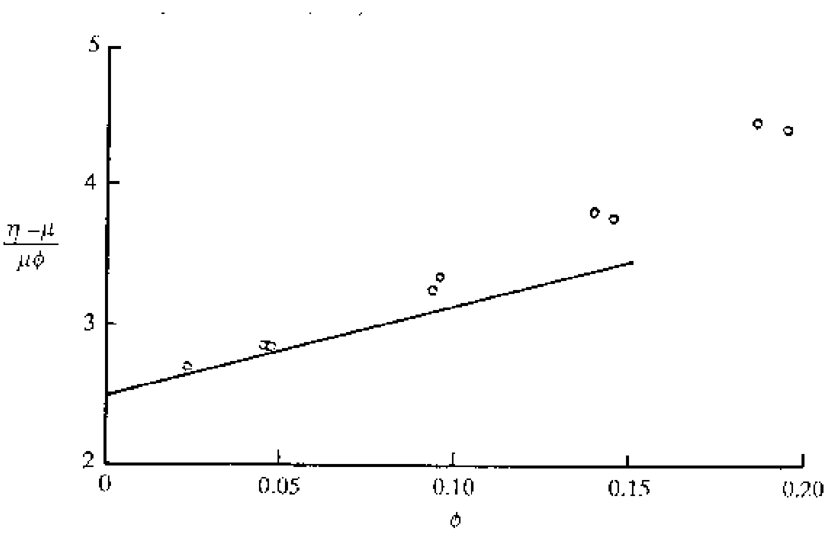

Figure 3: The data from [2, 3] verifying Equation 9

where viscous drag balances interparticle electrical repulsion. Here ζ is the surface charge density of the colloid, and ϵ is the dielectric constant for the solvent.

The effect of the charge particle interactions on the rheology can be calculated in much the same was as for uncharged rigid spheres. The result is an effective viscosity given by

$$\mu^* = \mu\left[1 + 2.5\varphi + 2.8\varphi^2\left(\frac{r_*}{a}\right)^5\right].$$

Since r_* is usually greater than a, the coefficient of the φ^2 term is much greater than the 6.2 found for the hydrodynamic interaction between rigid spheres, as illustrated in Figure 5. (This is Figure 14.19 from [4].) Changing the solvent ion concentration can have a large impact on the viscosity by changing the screening length κ^{-1}.

3.3 van der Waals Interactions

Van der Waals interactions allow aggregation of large, extended structures called flocs. Flocs are fractal structures with a typical dimension $d \sim 2.3$, which implies that they are packed more closely than a planar structure but less densely than a solid. If the flocs are small, they will tend to stick together after collisions but large flocs will be destroyed by strong flows. The size R of these flocs can be estimated by the following scaling argument. The number of particles of radius a in a floc is $N = (R/a)^d$ In equilibrium, the viscous forces (given by the Stokes drag formula) will balance the cohesive forces:

$$(6\pi\mu R)\ (\dot{\gamma}R) = F_b N\frac{a}{R},$$

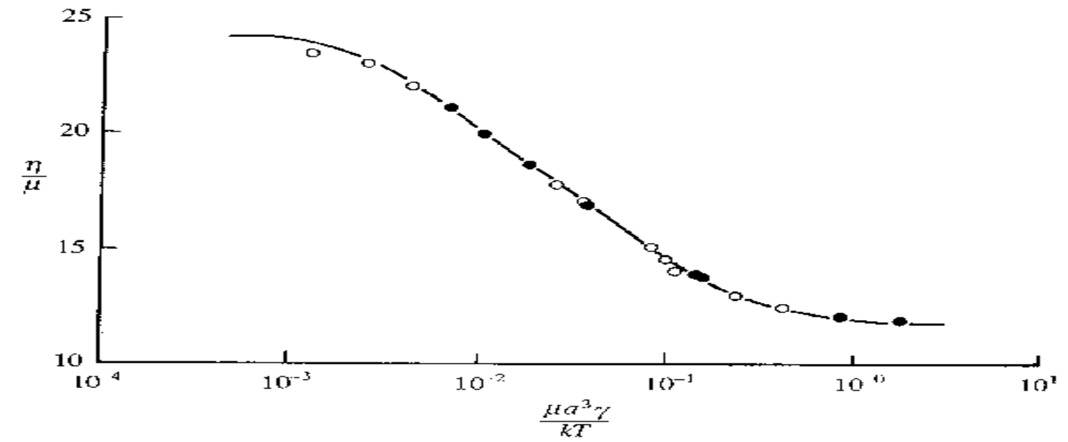

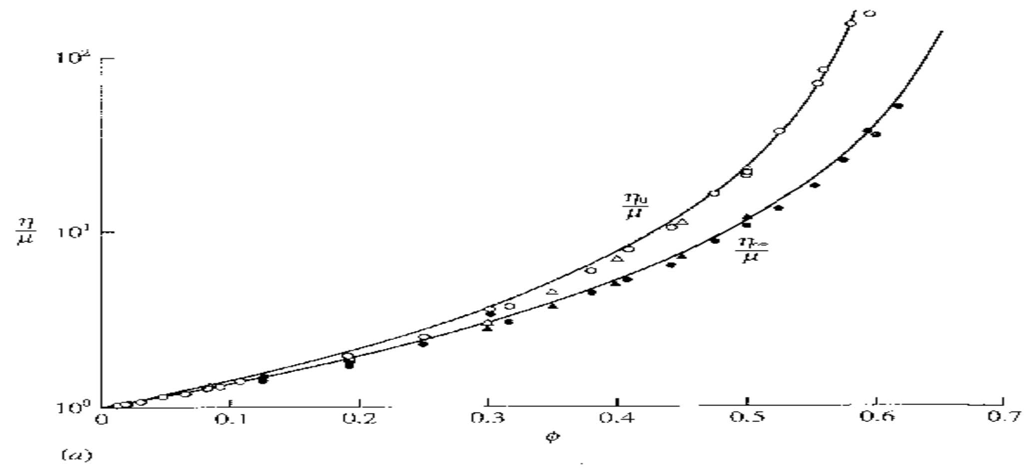

Figure 4: The shear thinning at high concentrations.

where F_b is the bond force and Na/R is the number of bonds per floc. Solving for R/a, we see that the volume fraction of the flocs is

$$\varphi_f = \varphi(R/a)^{3-d} = \varphi\frac{F_b}{6\pi\mu a^2\dot{\gamma}}.$$

The effective viscosity is simply the Einstein viscosity with φ_f replacing φ. Since $\varphi_f \sim 1/\dot{\gamma}$, suspensions of flocs exhibit strong shear thinning. The expression for φ_f is unbounded as $\dot{\gamma} \to 0$. However, physically, φ_f cannot be greater than one. Thus, at low shear rates the solution gels and has a yield stress $\sim (\varphi F_b/a^2)$.

3.4 Rigid Fibers

In contrast to dilute suspensions of rigid fibers, concentrated solutions cannot pack with random orientation if $\varphi r > 1$ because of topological constraints. (Here $r > 1$ is the aspect ratio of the fiber.) Instead, the fibers spontaneously align - this is called the nematic phase

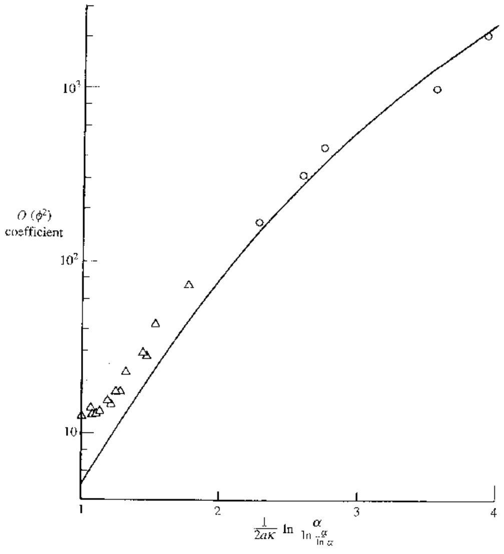

Figure 5: The coefficient of the φ^2 term in the effective viscosity

transition. As discussed in Lecture 5, the shear viscosity depends linearly on the aspect ratio and it can be large only when φr is large and the fibers are aligned. However, the extensional viscosity depends quadratically on the aspect ratio; it can be big even when $\varphi r < 1$ and the fibers are randomly oriented. Since the aspect ratio r of disks is less than 1, they cannot align randomly if $\varphi / r > 1$.

3.5 Drops

When the microstructure is deformable, the geometrical constraints are much less stringent and there is no jamming or locking of particles. During collision, the deformations lead to wider gap between the particles. Additionally, strong flow distorts the drops into cylinders with spherical end caps. These cylinders present a smaller collisional cross-section than a sphere of the same volume. This means that a suspension of drops is effectively 'dilute' even at a concentration of 30%. Because of this, blood works despite its high concentration of red blood cells.

4 Polymer chains

We have discussed microstructure without any internal structure. In the remaining part of the lecture, we will discuss various models for polymers, first for isolated polymers and then for entangled ones.

4.1 Isolated Polymers

The simplest model studied in the '40s is the bead-and-spring model, shown schematically in Figure 6. This model replaces a chain of N bonds each of length b with two spheres of

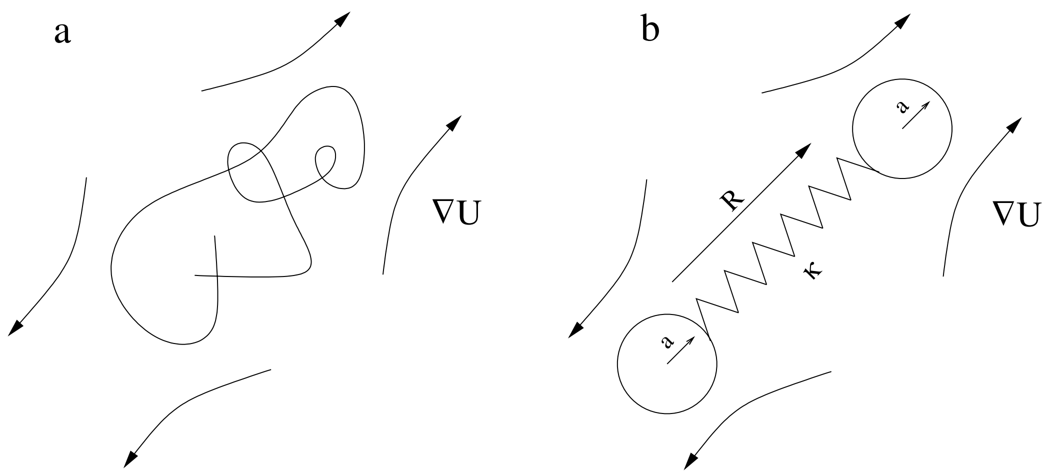

Figure 6: (a) A schematic drawing of polymer being distorted by the flow. (b) The bead-and-spring model to study the isolated polymer chains.

radius a joined by a spring of spring constant κ. Assuming that each bond is undergoing Brownian motion, we obtain the effective spring constant of $\kappa = 3kT/Nb^2$ and sphere radius $a = b\sqrt{(N/6)}$. If we denote by $\mathbf{R}$ the vector joining the two spheres, the Stokes drag on the spheres is $6\pi\mu a(\mathbf{R}\cdot\nabla\mathbf{u} - \dot{\mathbf{R}})$. Equating the drag force with restoring force $-\kappa\mathbf{R}$ of the spring, we obtain the time evolution of $\mathbf{R}$:

$$\dot{\mathbf{R}} = \mathbf{R}\cdot\nabla\mathbf{u} - \frac{1}{2\tau}\mathbf{R}, \qquad \text{where} \qquad \tau = \frac{\sqrt{6}}{\pi}\frac{kT}{\mu\left(N^{1/2}b\right)^3}.$$

The equation for the deformation tensor $\mathbf{A} \propto \mathbf{RR}$ is obtained as

$$\overset{\triangledown}{\mathbf{A}} = \frac{D\mathbf{A}}{Dt} - \mathbf{A}\cdot\nabla\mathbf{u} - (\nabla\mathbf{u})^T\cdot\mathbf{A} = -\frac{1}{\tau}\left(\mathbf{A} - \frac{Na^2}{3}\boldsymbol{\delta}\right).$$

The stress tensor is given by

$$\boldsymbol{\sigma} = -p\boldsymbol{\delta} + 2\mu\mathbf{E} + n\kappa\mathbf{A},$$

where n is the number density of the chains. This is the Oldroyd-B model. In a shear flow, μ is constant, the first normal stress depends quadratically on the strain rate, and the second normal stress is zero. As we noted in the second lecture, this model gives negative extensional viscosity when $\dot{\gamma}\tau > 1/2$ because the model allows the polymers to stretch indefinitely.

There are a number of (boring) refinements to the bead and spring model: Allowing the polymer to have a spectrum of internal modes just leads to a spectrum of relaxation times. Considering polydisperse molecular weight polymers smears out the relaxation time, but does not otherwise modify the model.

An extremely important refinement accounts for the fact that polymers cannot be extended indefinitely—they all have finite length. This is accomplished by modifying the spring force law so that the restoring force goes to infinity when the polymer is maximally extended. A common form for this force law is

$$\boldsymbol{F} = \frac{kT}{Nb^2} \frac{\boldsymbol{R}}{1 - R^2/L^2},$$

where $L = Nb$ is the total length of the polymer. This modification is called FENE for Finite Extension Nonlinear Elasticity.

Some other refinements are: inclusion of nonlinear bead friction; rotation of beads; nonlinear internal modes.

4.2 Entangled Polymers

A polymer in a concentrated solution is not free to move arbitrarily because neighboring polymer chains impose topological constraints. A class of models called the reptation models, first suggested by de Gennes in 1971[5], focuses on a single polymer which squiggles and squirms around other polymer chains, as shown schematically in Figure 7. Consider the

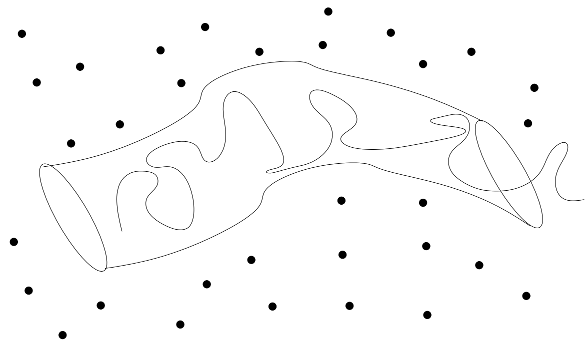

Figure 7: A polymer chain reptating through the tube formed by presence of other polymers

motion of a single polymer, keeping all the others fixed. Assuming that the chain diffuses along its length L with a diffusion constant D proportional to $kT/\mu L$, we see that the diffusion time scale is

$$\tau_d = \frac{L^2}{D}. \tag{10}$$

Since the molecular weight M is proportional to the length, the above equation implies that the diffusion time scale is proportional to M^3. But experiments discussed in Lecture 1 show this power to be 3.4. Attempts to capture this elusive 3.4 have lead to many refinements of this simple model. One of them (the A-BKZ model) considers the deformations with the mean flow of an effective tube containing the polymer [6]. A refinement of this refinement considers the effect of retraction of the polymer, which leads to an effective shrinking of the tube, along with the tube deformation. Another obvious refinement is to allow for the reptation of other polymers. The latter two theories have been combined together to give finally the correct power of 3.4 [7]!

Notes by Amit Apte and Christopher L. Wolfe?

References

[1] G. K. Batchelor, "The effect of brownian motion on the bulk stress in a suspension of spherical particles," J. Fluid Mech. **83**, 97 (1977).

[2] W. B. Russel, "A review of the role of colloidal forces in the rheology of suspensions," J. Rheology **24**, 287 (1980).

[3] F. L. Saunders, "Rheological properties of monodisperse latex systems," J. Colloid Sci. **16**, 13 (1961).

[4] W. B. .Russel, D. A. .Saville, and W. R. .Schowalter, *Colloidal Dispersions* (Cambridge University Press, Cambridge, 1989).

[5] P.-G. de Gennes, "Reptation of a polymer chain in the presence of fixed obstacles," Journal of Chemical Physics **55**, 572 (1971).

[6] M. Doi, "Explanation for the 3.4-power law for viscosity of polymeric liquids on the basis of the tube model," Journal of Polymer Science, Polymer Physics Edition **21**, 667 (1983).

[7] J. D. Cloizeaux, "Relaxation and viscosity anomaly of melts made of long entangled polymers - time-dependent reptation," Macromolecules **23**, 4678 (1990).